Measurement 123 (2018) 150–162

Contents lists available at ScienceDirect

Measurement

journal homepage: www.elsevier.com/locate/measurement

# Use of model-based library in critical dimension measurement by CD-SEM

Y.B. Zou[a], M.S.S. Khan[a], H.M. Li[b], Y.G. Li[c,*], W. Li[d], S.T. Gao[d], L.S. Liu[e], Z.J. Ding[a,*]

[a] Key Laboratory of Strongly-Coupled Quantum Matter Physics, Chinese Academy of Sciences, Department of Physics and Hefei National Laboratory for Physical Sciences at the Microscale, University of Science and Technology of China, Hefei, Anhui 230026, PR China
[b] Supercomputing Center, University of Science and Technology of China, Hefei, Anhui 230026, PR China
[c] Key Laboratory of Materials Physics, Institute of Solid State Physics, Chinese Academy of Sciences, Hefei, Anhui 230031, PR China
[d] National Institute of Metrology, Beijing 100013, PR China
[e] School of Optical Electrical and Computer Engineering, University of Shanghai for Science and Technology, Shanghai 200093, PR China

ARTICLE INFO

*Keywords:*
Model-based library
Critical dimension
Secondary electron
CD-SEM
Monte Carlo simulation

ABSTRACT

Model-based library (MBL) method, based on the fundamental physics of electron-solid interaction and Monte Carlo simulation of electron transport and secondary electron (SE) cascades, is an ideal algorithm in critical dimension (CD) metrology by CD-SEM, which exceeds the experiential structure characterization with SE profile curve. Particularly, comparing to the threshold method, the MBL method can extends to 3D metrology of CD by including many more geometrical structural parameters, such as, top CD, bottom CD, height and sidewall angles. In this work, we study the SE signal profile shape in CD metrology for the MBL method. The gate lines in trapezoidal cross section shape with arc corners are modeled for the simulation of SE linescans. The sensitivity of the SE intensity profiles to the different topographic parameters are investigated. In addition, the practical aspects of CD evaluation including pre-processing of experimental SE image and profile matching procedure are discussed. The work will be beneficial to the related standardization of CD measurement.

## 1. Introduction

Critical dimension (CD) is the minimum feature size in the wafer, which is one of the important quantities in dimension metrology. CD values represent the complexity level of manufacturing and need accurate measurement to meet the demand of strict dimensional control. The accuracy of CD measurement is challenging with very tight specifications in the process control for mask and wafer production. As a specialized length measurement instrument, critical dimension-scanning electron microscope (CD-SEM) has been used for CD measurement of nanostructures in the integrated circuit industry with its advantage of high resolution and fast imaging speed [1]. Secondary electron (SE) imaging is the mode used in the CD-SEM observation, which enables to detect the specimen structure with a high contrast. The CD metrology based on SE imaging consists of two steps, the pixel-based electron signal imaging and extracting CD values from the intensity profile by an appropriate algorithm [2].

An SE image is a point-by-point representation of SE intensity generated by a primary electron beam scanning over the specimen surface. SE intensity for a certain position of the specimen surface has a contribution from the nearby locations in the excited volume. In an SE image of nanometer-scale dense lines, the line edges are usually brighter than their surroundings by the edge effect that is resulted from a larger local emission area around an edge than elsewhere. Therefore, SE profile possesses characteristic peaks with certain expansion at an edge. The CD value determination depends on edge detection algorithm which assigns not only the abscissa of the edge location but also other structure parameters from the SE profile waveform. Because an SE image or a linescan profile is subjected to many influencing factors, such as, instrument condition, specimen structure and composition, the actual edge location within the expansion region is not known a priori [3–7].

Therefore, accurate CD metrology relies upon the full understanding of the relationship between SE image contrast and specimen property and experimental condition, and hence the developed algorithm to interpret an SE image contrast. Although CD-SEM has good instrumental advantages, it can still be subjected to a considerable error in CD metrology without a suitable CD determination algorithm. Experiential algorithms generally disregard the underlying physics of the SE signal generation and, hence, may cause an unpredictable, in some cases unacceptable large, bias. An experiential method for CD metrology considers the brightness threshold either artificially specified or determined by using a reference sample for some special cases [8]. The reported methods include the line fit algorithm [9], linear regression to

* Corresponding authors.
*E-mail addresses:* ygli@theory.issp.ac.cn (Y.G. Li), zjding@ustc.edu.cn (Z.J. Ding).

https://doi.org/10.1016/j.measurement.2018.02.069
Received 11 April 2017; Received in revised form 20 December 2017; Accepted 28 February 2018
Available online 23 March 2018

baseline, maximum derivative, sigmoidal fit [10] and multiple parameters profile characterization [11,12]. These experience-based algorithms have some limitations, e.g. arbitrary CD definitions [9] and single-valued CD; they could only exhibit usefulness under certain conditions but may produce wrong estimates under other conditions. In addition, for the development of new nanostructure manufacturing processes, such as fabrication of FinFETs, the metrology requires strict tolerances but also introduces additional critical process parameters, such as sidewall angle and height [3,13]. The dimension metrology based on SE image should have greater potential for 3D metrology; however, the empirical algorithms cannot adapt to this requirement.

To satisfy measurement tolerances and tight CD control requirements, the metrology algorithm based on physical modeling should be the best way. Monte Carlo (MC) simulation has played an important role in the progress of CD metrology algorithm [14–17]. In principle the model-based library (MBL) algorithm should be an ideal choice for CD-SEM metrology at advanced nodes [16]. MBL is a database of calculated SE linescan profiles by a MC simulation method which models the physical process of electron beam interaction with a specimen in the CD-SEM imaging; the simulation allows to establish a one-to-one relationship between the SE linescan profile and its specimen geometric structure and beam condition. Davidson et al. have firstly put forward the idea to develop a measurement algorithm that is based directly on simulated SE image or linescan profile [18,19]. Gorelikov et al. have used an off-line MC simulation library and in real time compared to the measured intensity profiles in CD-SEM at low and ultralow landing energies, with a significantly better agreement with other metrology technologies than the traditional CD metrology algorithms [20]. Frase et al. have reviewed the existing MC simulators for simulation of SE image and shown how the model-based methods can be applied to test and validate newly developed CD edge metrology algorithms like the mathematical algorithms [21,22]. Villarrubia et al. have calculated SE images for varying structural parameters and used them to assign the edge shape. The measurement results from a top-down SEM image agreed very well with cross-sectional SEM observation and had better same-site repeatability than the traditional techniques [3,14,23–25]. Tanaka et al. have evaluated the linewidth measurement ability of the MBL matching technique and also investigated the influence factors [26–28]. Babin et al. have simulated SE signals for varied linewidth, which were intended to be a guide for regular image processing threshold adjustment. It was found that any fixed threshold results in CD errors when feature size varying so that the CD error bias is not a constant, which indicates that there is no single correct threshold [15,29]. Karabekov et al. have developed a MC simulation program to model SE signals, and deduced the edge location of the line structure by correlating features of the simulated linescans [30]. Ciappa et al. have proposed a MC simulator tool for the quantification of CD-SEM images and emphasised on the scattering models for the low-energy range [31]. Li et al. have performed a MC simulation for a comprehensive understanding of the influencing factors to CDs [32]. By using the existing MC models, the MBL method has also been applied to CD metrology of different materials [33–37].

In principle, the MBL method should be the most accurate algorithm due to its one-to-one relationship between the signal intensity profile and the geometry structure; a number of CD parameters could be assessed from a direct comparison of the SE intensity profile with that of a simulated one saved in a pre-prepared MBL database. The method can take into account the influencing experimental factors as much as possible, including electron beam conditions and sample specifications (chemical composition, geometry parameters and the surrounding feature of a structure). However, in practice, one has to consider its limitation on the resource requirement to exclude those parameters that are insensitive for SE linescan profile and may have less importance to CD metrology. Furthermore, although there is a one-to-one relationship between an image and a modeling structure it may still be hard to distinguish within experimental error range of signals the different cases that having the quite similar shape of SE linescan profiles but corresponding to different values of the experimental parameter set.

MBL method requires great computation efforts to construct a calculation database due to lots of different experimental parameters involved. The reliability and implementation of the MBL method for CD metrology rely on the MC simulation modeling of the complex process of SEs generation and high-efficiency computation, respectively. Noted that with the improvement of SE generation model in recent years, the MC method becomes more sophisticated and mature. For MC simulation, various physical models have been developed to deal with electron elastic and inelastic scattering as well as SE generation under various approximations. The early approach for electron inelastic scattering and associated SE generation based on the continuous slowing down approximation [18–21,23,24] has now been replaced by a more exact dielectric functional approach which can provide consistent result in agreement with experiment without fitting parameters [3,25,38–40]. The influence of different MC models to the CD metrology has been carefully analyzed [25]. Reasonable physical model for SE image simulation, sophisticated sample geometric modeling and high-efficiency simulation method are fundamental demands to construct a library practically useful in CD metrology.

Here we shall employ the up-to-date MC physical modeling that is currently used for SEM applications for metallic and semiconductor materials, which allows a direct simulation of cascade SE production and emission without fitting parameters. In our previous works, a MC simulation program for modeling of electron-solid interaction, SE generation, SE emission and cascade have developed [38,39,41–46]. Furthermore, a calculation has been done to investigate the influence of various experimental factors to the CD-SEM image contrast in detail, advancing a step towards the realization of MBL method [32,47,48]. With the 3D specimen model implemented an arbitrarily shaped structure can be constructed, and be defined with some structural parameters for regular shapes; a spatial segmentation acceleration algorithm was used in such 3D MC simulation to reduce the computation cost.

Obviously, the more stringent specification of specimen structure is, the greater size of specimen database and calculation cost are. It is then necessary to study the sensibility of SE linescan waveform to the structural parameters. In this paper, we have investigated the relationship between SE intensity distribution and a line structure in trapezoidal cross section shape with arc corners. The influence from surrounding features of a structure is also considered in the signal collection, which is necessary for the practical realization of MBL method and needs to be studied more deeply. Furthermore, we shall discuss some practical aspects of CD evaluation towards standardization of measurement procedure including pre-processing of experimental SE image and profile matching. The metrology capability and limitations of CD-SEM with regular image processing are identified. As the rapid development in the semiconductor industry towards smaller sizes urges the building of the comprehensive MBL method, the goal of this work is to improve the ability of the MBL method for the future development of technical tools federating MBL.

## 2. Models of MBL simulator

In SEM observation, the incident electrons strike the surface of the specimen, then a series of elastic and inelastic scattering process takes place inside the specimen; for incident electrons and generated SEs the scattering process and electron trajectories are simulated until they either are absorbed by losing their kinetic energies or leave from the specimen surface. All the simulated electrons, primary electrons and SEs, can generate further cascade SEs along their trajectories in the target (Fig. 1). A MC simulation package, termed as MBL simulator, is consisted of several components for specification of the physical modeling and related parameters, i.e. the electron probe module, the beam-sample interaction module, SE signal detection module, and the

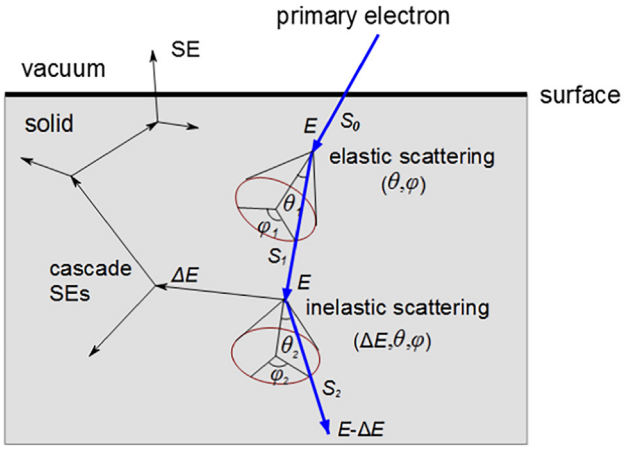


**Fig. 1.** Schematic diagram of Monte Carlo simulation of electron scattering in the solid and the associated SE cascade generation process.

specimen geometrical structure module.

### 2.1. Electron probe module

The SE signal is decisively influenced by tool setup and specimen structure [7], and the resolution of imaging by a CD-SEM depends on the electron probe size and on the interaction volume of electrons within a specimen [49–51]. An electron probe module should provide the sufficient information about the incident electrons in a simulation, i.e. primary energy, incident angle and probe model.

In many cases of practice, especially with nanometer-scale structures, the stray tilt of the electron beam has to be considered [52]. The primary electron beam is usually not perfectly perpendicular to the sample, but deviates from that within several degrees in two planes. Two tilt angles, $\vartheta_x$ and $\vartheta_y$, describe the angles of incidence of electron beam with respect to surface normal, respectively, in *xz*-plane and *yz*-plane where the *y*-direction is defined along the line in Fig. 4.

We do not require an electron probe model to reproduce sufficiently real electron optics [50] but that to reasonably describe the spatial distribution of the incident electron beam landing on the specimen surface. The behavior of the electron beam, such as, intensity distributions and optimum focus positions, can be described by a series of parameters in various models [3,53–57]. Two types of the probe model are adopted in our simulation of SE images, that is, the Gaussian beam model [32] and a focusing beam model [53].

In an ideal electron beam case, the probe has vanishing landing spot size on the surface of a specimen; then the simulated ideal image has the highest spatial resolution. For a Gaussian beam, it is assumed that the probe size $d_p = 2\sqrt{2\ln 2}\,\sigma_b$ is constant vertically when scanning over the sample surface; the image resolution is then unrelated to specimen structure. The 2D image intensity can be obtained simply by a convolution of the simulated image intensity for an ideal beam with the Gaussian distribution,

$$G(r|\sigma_b) = \frac{1}{2\pi\sigma_b^2}\exp\left(-\frac{r^2}{2\sigma_b^2}\right), \tag{1}$$

where $r$ is radial distance in *xy*-plane from the probe center. Here, an electron beam with finite landing spot size is characterized by the standard deviation ($\sigma_b$), and the probe size is the diameter of the circle that contains 50% of the total probe current. For 1D linescan profile, the convolution is carried out with the Gaussian distribution,

$$G(x|\sigma_b) = \frac{1}{\sqrt{2\pi\sigma_b^2}}\exp\left(-\frac{x^2}{2\sigma_b^2}\right). \tag{2}$$

To minimize the library size, it is recommended to simulate SE linescan profiles only for an ideal electron beam; the Gaussian distributions for different probe sizes can be later used in a convolution procedure to derive linescan profiles in MBL curve matching procedure.

However, the Gaussian beam model cannot take into account of electron beam focusing effect which may be significant for vertically large structures. In this case, the spatial distribution of incident electrons arriving at the specimen surface is related to beam focusing condition. Thus, the real beam shape and size vary with the landing position, which in turn affect an SE image [55]. To analyze the effect of beam shape to linewidth measurement, a focusing beam model with aberration effect included may be used to simulate SE linescan under different focusing conditions. Four parameters, nominal probe size or effective beam width $d_p$, working distance $d_s$, aperture angle $\alpha$ and focusing distance $d_f$, are used in this model to characterize the incident beam [53]. The focusing position is measured from the specimen top surface where it is defined as the just-focus position (i.e. $d_f = 0$), while $d_f < 0$ and $d_f > 0$ correspond to under-focus and over-focus cases, respectively, where the vertical coordinate is positive along the beam incidence direction. By the focusing beam model, an incident electron trajectory with its incident direction and landing position are determined by random sampling two horizontal positions in aperture plane and focal plane from Gaussian distributions and connecting them as a straight ray towards the landing surface (Fig. 2). At the aperture plane and focal plane, the beam widths are given respectively by $d_s\tan\alpha$ and $d_p$. This modeling is simpler than that described in Ref. [53] but can result in a Gaussian profile at a landing surface while the beam width is varied with the landing position, as we required. The obtained MBL curves are directly matched with the measured one without convolution. Focusing beam model excels Gaussian beam model in accuracy of description of SE linescan profiles by adding further three parameters but enlarging greatly the MBL data file size.

### 2.2. Beam-sample interaction module

Beam-sample interaction module is the core component of a MBL simulator. After striking the specimen surface the incident electrons penetrate into the solid and the complex electron-solid interaction process is then initiated, which is separated into two categories of elemental electron interactions with atomic nuclei and electrons for electron elastic and inelastic scattering, respectively. The excitation and emission of SEs are the results of the fundamental scattering process inside the solid specimen. The MC simulation of CD-SEM imaging process is based on a physical modeling for theoretical description of the electron-solid interaction under various approximations [25,58].

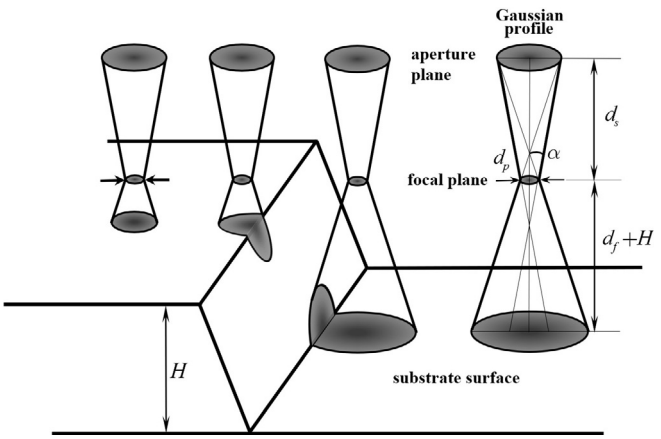


**Fig. 2.** Schematic diagram of focusing electron probe shape at different landing positions of a line structure. α is the convergence angle, $d_s$ is the working distance, $d_f$ is the distance between focal plane and the top surface, $H$ is height, $d_p$ is the effective beam width or the diameter of least confusion disc along the beam axis.

Here, we employ the up-to-date MC physical modeling currently used in SEM image simulation [32,39,53,59,60]. For electron elastic scattering the Mott's differential cross section [61],

$$\frac{d\sigma_e}{d\Omega} = |f(\theta)|^2 + |g(\theta)|^2, \tag{3}$$

is calculated with the Thomas-Fermi-Dirac atomic potential [62], where the scattering amplitudes, $f(\theta)$ and $g(\theta)$, as function of scattering angle $\theta$, are calculated by a partial wave expansion method [63,67]. As Mott's cross section is not represented by a specific analytical expression, the calculated numerical values of the differential cross section are usually pre-stored into a data file for a MC simulation.

Electron inelastic scattering induces the excitation of electrons in the solid, which is largely less localized than the elastic scattering and is mainly limited to small scattering angles; it is then associated with the energy loss of electrons. Based on the fundamental physics of electron inelastic scattering there are different inelastic interaction mechanisms related to the SE generation, including inner-shell excitation, single electron excitation and plasmon excitation. The unified treatment of these inelastic channels is provided by the dielectric functional approach, which handles as well the SE production in an electron inelastic scattering event.

For an electron with kinetic energy $E$ moving in a solid, the differential inverse electron inelastic mean free path (DIIMFP) is given by,

$$\frac{d^2\lambda_{in}^{-1}}{dqd\omega} = \frac{\hbar}{\pi a_0 E}\mathrm{Im}\left\{\frac{-1}{\varepsilon(q,\omega)}\right\}\frac{1}{q}, \tag{4}$$

where $\lambda_{in}$ denotes electron inelastic mean free path (IMFP), $a_0$ is the Bohr radius, $\hbar\omega$ and $\hbar q$ are energy loss and momentum transfer of moving electron, respectively. $\varepsilon(q,\omega)$ is the dielectric function of the material; $\mathrm{Im}\{-1/\varepsilon(q,\omega)\}$ is called energy loss function which determines the weight of electron inelastic scattering channels. The energy loss and the associated SE production in individual scattering events are treated by a MC random sampling. The full Penn algorithm (FPA) [64] for extrapolating the optical energy loss function $\mathrm{Im}\{-1/\varepsilon(0,\omega)\}$ into $(q,\omega)$-plane yields a better agreement than the single-pole approximation (SPA) on SE yields and energy distribution curves to be compared with experimental measurements, particularly for free-electron-like materials whose bulk plasmon peak dominates the energy loss function [38]. Hence, in this work the FPA is employed to calculate energy loss function, which is expanded according to Lindhard dielectric function $\varepsilon_L(q,\omega;\omega_p)$ as follows:

$$\mathrm{Im}\left\{\frac{-1}{\varepsilon(q,\omega)}\right\} = \int_0^\infty d\omega_p g(\omega_p)\mathrm{Im}\left\{\frac{-1}{\varepsilon_L(q,\omega;\omega_p)}\right\}, \tag{5}$$

where the expansion coefficient $g(\omega)$ is related to the optical energy loss function by $g(\omega) = (2/\pi\omega)\mathrm{Im}\{-1/\varepsilon(\omega)\}$ [64], and the optical data are taken from an experimental database. The advantage of this modeling is that the complex electronic excitation in real materials is more accurately described through the use of optical data as the input to a MC simulation. The sufficient dielectric data for $\varepsilon(0,\omega)$ or optical constants in the loss energy range of $10^0$–$10^4$ eV experimentally measured by optical methods are available and compiled for many metals and semiconductors [65,66].

By FPA the total energy loss function is the summation of the two parts contributed by single electron excitation and bulk plasmon excitation, respectively, as:

$$\mathrm{Im}\{-1/\varepsilon_L(q,\omega)\} = \mathrm{Im}\{-1/\varepsilon(q,\omega)\}_e + \mathrm{Im}\{-1/\varepsilon(q,\omega)\}_{pl}. \tag{6}$$

Then the treatment of SE generation by FPA needs to consider two distinct mechanisms, i.e. single electron excitation and via plasmon decay [38]. The dielectric functional formalisms (FPA and SPA) are better than the stopping power equation approach in continuous slowing-down approximation and the other discrete scattering channel approach in the description of electron inelastic scattering and secondary electron signal generation; and FPA is superior to SPA.

### 2.3. SE signal detection module

According to the individual electron inelastic scattering model, the energy loss of a moving electron is transferred to a knock-on electron and to cause a SE generation. The moving direction of the generated SE is assumed to be isotropic. An excited SE will undergo similar elastic and inelastic collisions as primary electrons and cause generation of multiple lower energy SEs; this is the so-called cascade production process of SEs. Only those electrons with kinetic energy above the vacuum level can be emitted into vacuum, and among them whose energies are lower than 50 eV will be counted as true SE signals. When reaching the surface from the interior of a specimen for emission, an electron is refracted by the potential barrier because the surface barrier affects the energy and angular distribution of emitted slow electrons. There are two approaches for transmission function: The classical one as a step function only requires that the kinetic energy is higher than the inner potential, while the quantum mechanical representation gives the varied emission probability depending on the kinetic energy $E$ as well as the ejection angle $\psi$ measured from surface normal [67,68],

$$T_q(E,\psi) = \begin{cases} \frac{4\sqrt{1-U_0/E\cos^2\psi}}{1+\sqrt{1-U_0/E\cos^2\psi}}, & \text{if } E\cos^2\psi > U_0; \\ 0, & \text{otherwise.} \end{cases} \tag{7}$$

The kinetic energy measured from the vacuum level is lowered by the inner potential $U_0$.

SEs emitted from the sample obey cosine law of angular distribution. They travel in straight lines in a space free of the electric field and may re-enter into the sample if they meet neighbouring structural surfaces in their way of movement. In this case, the SE signal is shadowed and cannot be counted by a detector, thereby resulting in SE yield reduction. However, the low-energy emitted SEs can be collected with high efficiency by a detector biased to a positive potential of several hundred volts to prevent the loss of signals. A quantitative detector model is thus helpful for taking account of the shading effect in CD-SEM simulation and also the unknown effect of detector geometry on signal collection.

The detection module records statistics of final SE signals emitted under two modes, i.e. full extraction and non-extraction, from the incident location of an electron beam scanning over specimen structure. It is practically useful to compensate the unknown detector property and detection efficiency for a particular type of CD-SEM instrument by using a parameter, $p_{ext}$, representing the degree of extraction by an external field [21]. The value of $p_{ext}$ is between 0 and 1, where $p_{ext} = 0$ represents the case of non-extraction or full shading effect, and $p_{ext} = 1$ the case of full-extraction or non-shading effect by a sufficiently strong external electric field. In the non-extraction mode, escaping SEs from the surface are supposed to travel in straight lines and have a chance in their paths to enter a neighbouring structure, which can be a neighbouring line, substrate or a nearby local rough surface. Their final fate may either be absorbed or excite more SEs emitted from the neighbouring structure. In the full-extraction mode, a SE is detected as soon as it is emitted from the local sample surface without a chance to enter a neighbouring structure. In the partial extraction mode, SE signals are extracted with the probability of $p_{ext}$ and the corresponding image intensity is given as, $I = (1-p_{ext})I_0 + p_{ext}I_1$, where $I_0$ and $I_1$ represent the intensity of non-extraction and full-extraction, respectively. Clearly, for a MBL construction only $I_0$ and $I_1$ are necessary to be included, while the partial extraction intensity can be later calculated in MBL curve matching procedure.

### 2.4. Specimen geometrical structure module

A model of specimen structure is specified by the geometrical

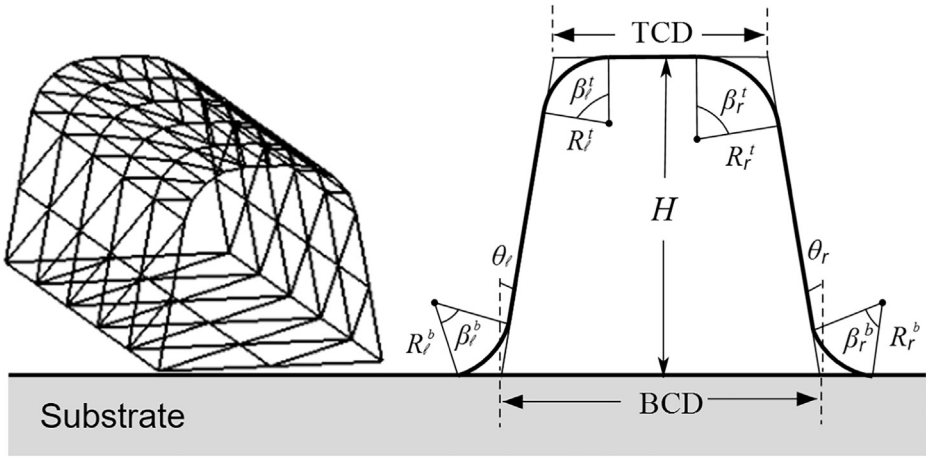


**Fig. 3.** The schematic diagram of parameters specifying a single line structure: $\theta$ is the sidewall angle, β is circular angle and $R$ is arc radius. The subscripts, "$l$" and "$r$", represent the left- and right-sides respectively; and the superscripts, "$t$" and "$b$", represent the top and bottom respectively. Left figure shows a 3D geometrical representation of a line with arcs and smooth surface, which is constructed by a finite element triangle mesh.

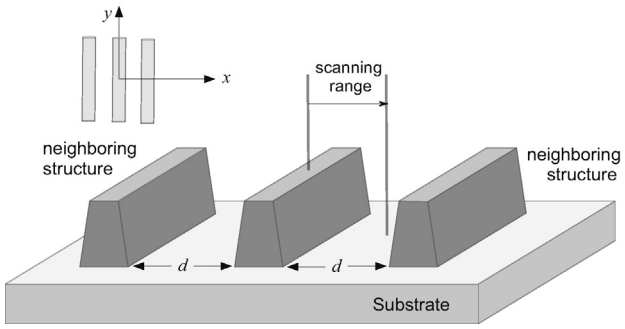


**Fig. 4.** The line structure is made of three identical lines; the simulation of scanning range of primary electrons needs to be performed only for the central line.

boundary with the surface topography and the materials included. The SE yield relies on the atomic number of the specimen [68]. For a MC simulation, the elemental composition of the specimen is specified prior and following it, other material properties including density, work function, Fermi energy (and band gap for semiconductors and conductivity for insulators [69]) are default inputs.

By the MBL method, the CD metrology aims not only to evaluate the linewidth but also all the other parameters of the topography, so that the simulation results can be used to predict and restore the 3D nanostructure information. Consequently, full description for geometry and appropriate construction method of the specimen is necessary. Fig. 3 is the schematic cross section of a single line structure with a smooth surface, where we have omitted the parameters characterizing a rough surface [39]. The parameters describing the line structure model are as following: top CD (TCD), bottom CD (BCD), height ($H$), right- and left-sidewall angles (SWA: $\theta_r$ and $\theta_l$), right- and left-top circular angles (TCA: $\beta_r^t$ and $\beta_l^t$), right- and left-top arc radiuses (TAR: $R_r^t$ and $R_l^t$), right- and left-bottom circular angles (BCA: $\beta_r^b$ and $\beta_l^b$), right- and left-bottom arc radiuses (BAR: $R_r^b$ and $R_l^b$), where BCD is not an independent variable and can be obtained from TCD, $H$ and SWA. Single line structure can be either symmetric or asymmetric. The ideal trapezoid shape is the simplest geometry when the arc radius is vanishing. The number of independent parameters for geometry description of a line is 8 in the symmetric case, while it is 13 in the asymmetric case. The asymmetric case hence greatly enlarges the volume of MBL data. In order to reduce the cost of MBL resource, we recommend to approximate the asymmetric case by joining two half parts of simulated symmetric data for different structure parameters (SWA, TCA, TAR, BCA and BAR) but with the same TCD and $H$.

Different methods can be used to build the expected specimen geometry or surface topography, for example, constructive solid geometry (CSG) [43,59], finite element triangular mesh (FETM) [39,70], tetrahedral mesh method [3] and height maps which is a 2D array of heights on a regularly spaced $x$- and $y$-grids [40]. FETM method is more adaptable to the construction of specimen topography, especially for structures with circular angle and rough surface. A single line geometry with a smooth surface, which is constructed by the FETM, is depicted as an inset in Fig. 3. Considering the complexity of treatment of electron scattering near the boundary as well as the optimization of simulation, FETM method is recommended for the generation of specimen geometric model for MBL database construction.

SE yield increases with the incident angle of the beam in relative to the local surface normal, so the surface-tilt is one of the main sources of topographic contrast. In addition, the shading effect associated with SE signal detection cannot be ignored. This is because the SE image of line structure is not only affected by the topography of the specimen to be measured but also incorporates the influence of neighbouring features. Therefore, one needs to consider the line structure as composed of three identical lines, with spacing $d$, sited on the same substrate (Fig. 4). Then the geometric parameters are totally 6, in addition to two parameters for specifications of materials of line and substrate. Only the MC simulation for the central line is necessary, as indicated by the scanning range in Fig. 4, while the two lines aside are used to take into account the shading effect in the non-extraction and partial extraction modes of SE signal detection. To save resources, in fact, the scanning range for simulation can be only the half part of the central line. Thus, for MBL data construction the origin of horizontal coordinate of the line image is set to the center of a line, and the scanning range is set as $(0, d/2)$. In a MC sampling procedure of flight length, it is necessary to have a quick judging of the intersection of an electron flight path with a surface or a boundary between two parts of materials in a specimen. For this, the space subdivision method is helpful to accelerate the calculation [32].

## 3. Results and discussion

### 3.1. Monte Carlo simulation of MBL data

A MBL database for CD evaluation is produced by a comprehensive MC simulation with a MBL simulator for a given combination set of experimental parameters. Input for a MC simulation includes parameters of the geometric structure (i.e. top CD, height, sidewall angle, circular angle, arc radius and spacing), material properties (e.g. elemental composition, density, optical dielectric function and electronic properties), parameters of electron beam (e.g. energy, tilt angles and optional beam focusing parameters). Among them, only some are the real independent parameters for MBL database construction as listed in Table 1, while others are not independent variable, for example, dielectric function is related to the specification of material.

**Table 1**
List of MBL module parameters.

| Module | Electron probe | Beam-sample interaction | Signal detection | Specimen geometric structure |
|---|---|---|---|---|
| Parameters (symbol) | Primary energy ($E_p$)<br>$x$- and $y$-tilt angles ($\vartheta_x$, $\vartheta_y$) Probe size ($d_p$) Working distance ($d_s$)<br>Aperture angle ($\alpha$) Focusing distance ($d_f$) | Line material<br>Substrate material | Extraction ratio ($p_{ext}$) | Spacing ($d$)<br>Top CD<br>Height ($H$)<br>Right- and left-sidewall angles ($\theta_r$,$\theta_l$)<br>Right- and left-top circular angles ($\beta_r^t$,$\beta_l^t$)<br>Right- and left-bottom circular angles ($\beta_r^b$,$\beta_l^b$)<br>Right- and left-top arc radius ($R_r^t$,$R_l^t$)<br>Right- and left-bottom arc radius ($R_r^b$,$R_l^b$) |
| Number of parameters | 4 (ideal or Gaussian model)<br>7 (focusing model) | 2 (effective) | 1 | 8 (symmetric)<br>13 (asymmetric) |

In a MC simulation, the incident electrons penetrate the surface of the specimen into the bulk, and then a series of elastic and inelastic scattering processes take place inside the specimen. The electrons are absorbed by losing their kinetic energies down to below inner potential or leave from the specimen surface. All the simulated electrons, either primary electron or SEs, can generate further cascade SEs via inelastic scattering along their trajectories in the target. For each scanning point, i.e. the image pixel, a certain number of, usually thousands at least to ensure good statistics, incident electron trajectories are necessary for a MC simulation of a linescan profile in an image. Such a calculated SE signal intensity curve, i.e. SE yield as a function of beam scanning position, is recorded into a MBL as an entry of library data. The SE yield is obtained as the number of emitted SEs divided by the number of incident electron trajectories. This simulation is repeated for the designed value range of the input parameter set to form a MBL database.

The typical calculation time for one library entry by a MC simulation is in the order of hours, which relies on hardware and computation conditions. For example, in this paper, for 3 keV primary electrons incident on an Au/Si sample with 50 horizontal scanning points (i.e. one database entry) with one hundred thousand incident electron trajectories for each scanning point, the simulation time is about 2 h by using 10 core parallel computations.

The calculation results presented here are all for normal incidence of primary beam, i.e. $\vartheta_x = \vartheta_y = 0$, and for a line structure without bottom arc, i.e. $R_r^b = R_l^b = 0$. Fig. 5 shows the influence from surrounding features of a structure, as the shading effect to the SE detector. Three Au gate lines are used to simulate SE linescan under full-extraction and non-extraction modes. Because of the edge effect, the peaks appear around two outer edges of the gate line, and they become more intensive by the full-extraction. For the central line, the SEs yield is reduced at edges under the non-extraction detector mode by the shading effect.

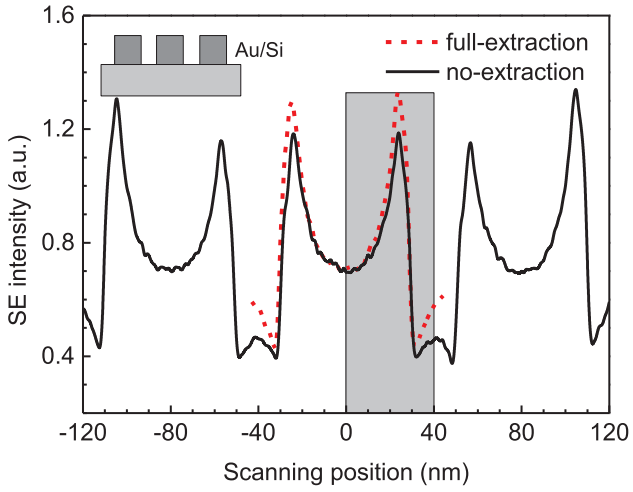


**Fig. 5.** Comparison on the simulated SE linescans between the full-extraction mode and non-extraction mode for Au gate lines (TCD = 50 nm, SWA = $0^0$, $H$ = 60 nm and $d$ = 20 nm) on a Si substrate. The primary energy is 1 keV. The shaded area represents the effective horizontal scanning range for a MBL database construction.

In order to study the influence of different structure parameters, single Au gate line on a Si substrate is considered for simulation of SE intensity distribution. In the simulation, beam conditions are kept the same in different cases; the incident energy is 3 keV and the beam size is 2 nm by the Gaussian beam model. Fig. 6 shows examples of the simulated SE linescans by changing those listed CD parameters. The position of SE intensity bloom is seen sensitive to TCD and SWA in Figs. 6(a) and 6(b), respectively. In Fig. 6(c) , the significant change of peak intensity has been found due to the change of height of the Au line. When normalized with peak maxima, the bloom range of the SE profiles is dramatically altered by $H$. The main reason is that when $H$ is small, a portion of the primary electrons will penetrate through the Au-line into the Si-substrate while the SE production in Si is lower than that in Au. Figs. 6(d) and 6(e) show the effect of top arcs. Introducing arc results in the broadening of the edge bloom because the SE emission intensity obeys inverse cosine law as $1/\cos\vartheta$, where $\vartheta$ is the incident angle of the primary beam respect to local surface normal. As the linescan waveform is also sensitive to the top arcs, it is recommended to include the top arc and arc radius as necessary parameters in MBL. However, the bottom arcs are not so important and will be excluded.

Fig. 7 shows the simulated SE linescan profiles of an Au trapezoidal gate line on a Si substrate under different focusing beam conditions. In excessive over-focus and under-focus cases, SE linescans have lower contrast and are more widely broadened. The sharpest edge contrast happens when the focusing position falls in the vertical position range between the top surface ($d_f = 0$) and the substrate surface ($d_f$ = 60 nm). In just-focus case ($d_f = 0$), the aperture angle has no obvious effect on linescan contrast, except on the intensity near the specimen bottom. In addition, the simulated SEs profile with a Gaussian electron beam is shown (for the case of $\alpha = 0°$), which is similar to the result of focusing beam with an aperture angle of $\alpha = 5°$ in Fig. 7(c). Condition of electron beam focusing is an influencing factor worthy to be included in linewidth measurement.

The angle of the primary electron beam respect to local surface normal is defined as the incident angle $\vartheta$, i.e. the stray tilt angle of the beam. Fig. 8 shows effect of incident angle of primary beam with Gaussian distribution on the SE emission. SE linescan profile changes with the incident angle at the structure edge.

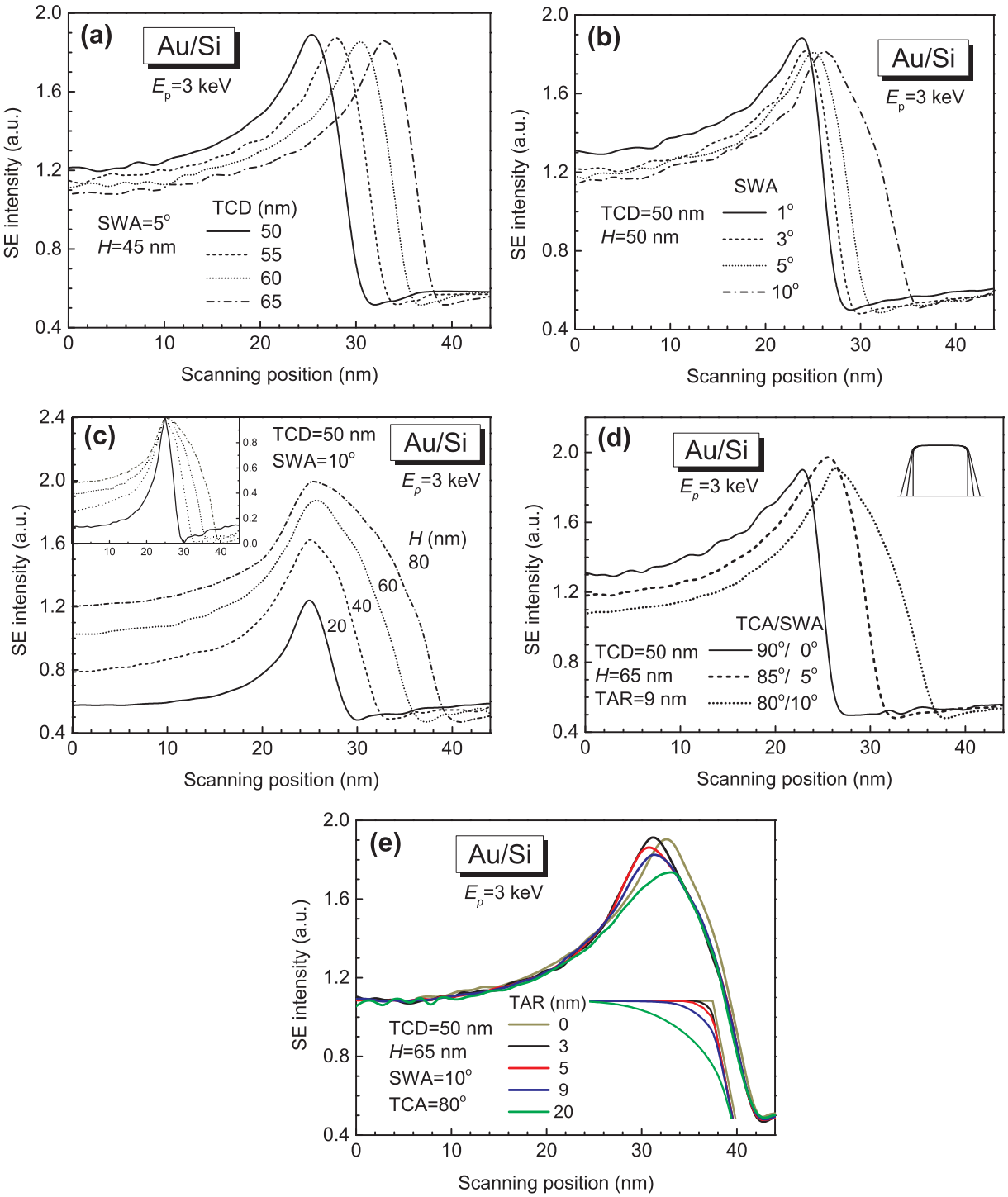


**Fig. 6.** Comparison on the simulated SE linescans for Au gate lines with different structure parameters by changing: (a) TCD; (b) SWA; (c) *H*; (d) TCA/SWA; (e) TAR.

### *3.2. Construction of MBL*

#### *3.2.1. Ingredient and structure of MBL*

The structure for the data file uses the hierarchical model as well as the relational model (Fig. 9). The hierarchical model is used to establish the relationship of the data for the navigation of beam and detection parameters, while the relational model is used to establish the connection between the structural parameters of the specimen and SE linescan curves.

All data in the database are stored in binary format to ensure the accuracy of data and to reduce the storage space. The data file should contain a head for the specification of number of grid points, *K*, and grid size, $L_g$ (in unit of nm), in order for the calculation of grid values along the scanning direction in *x*-coordinate, number of chemical compositions, number of primary energies (and number of beam focusing parameters, which is 2 for focusing beam and 0 for Gaussian beam. Values of structural parameter and SE linescan profile data, $I_i^{\mathrm{MBL}}$ ($i$ = 1,2,...,$K$), are stored sequentially in the relational model. Reasonable design of data structure and optimized matching algorithm will guarantee the MBL method to be realized, which can also overcome the limitation of the resource cost. In addition, due to the statistical nature of MC method the simulated linescan curve contains

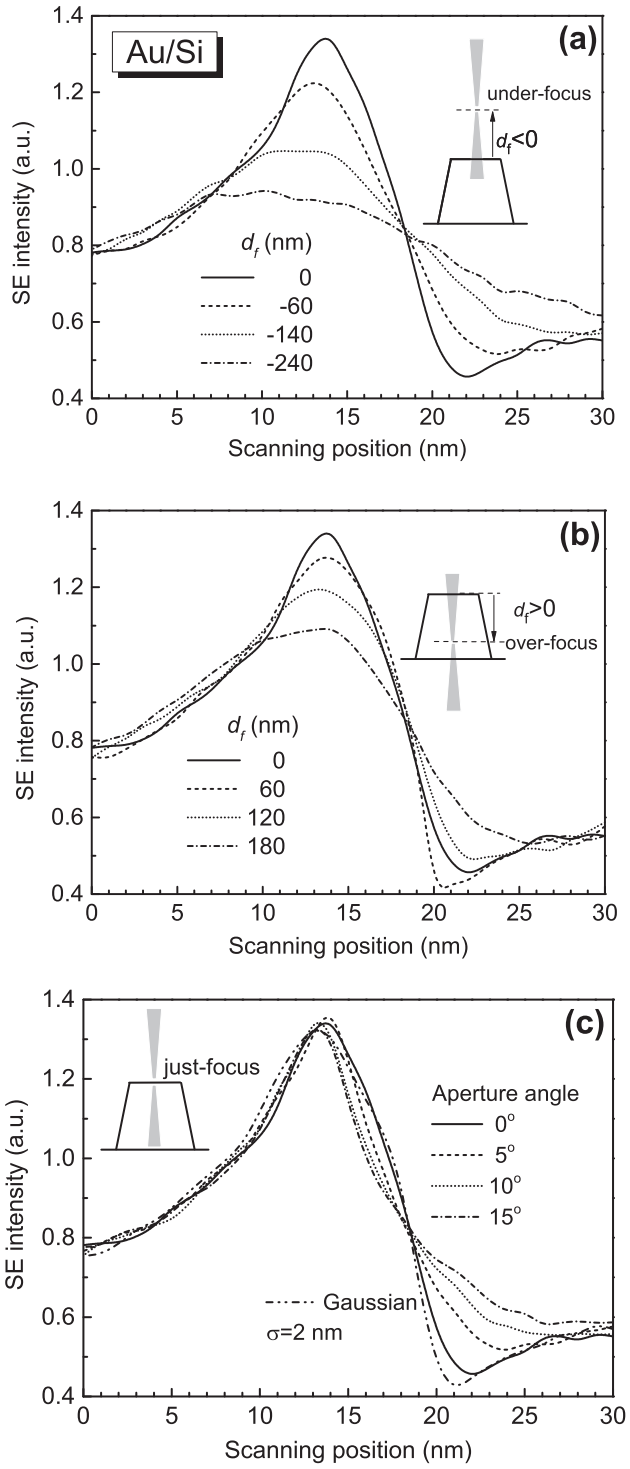


**Fig. 7.** The simulated SE linescan profiles of an Au gate trapezoidal line on a Si substrate under different electron focusing beam conditions: (a) under-focus; (b) over-focus; (c) just-focus but with different aperture angles; the result by a Gaussian beam model (probe size of 2 nm) is also plotted for a comparison. The input structure parameters are: $H$ = 60 nm, TCD = 50 nm, SWA = $5^0$; the primary energy is 1 keV and aperture angle is $5^0$.

unavoidable noise, particularly for fine scanning grid and a small number of primary trajectories. This noise may cause unreasonable normalization of intensity in MBL matching procedure. A suitable data smoothing is preferred before storing the simulated data into a MBL data file.

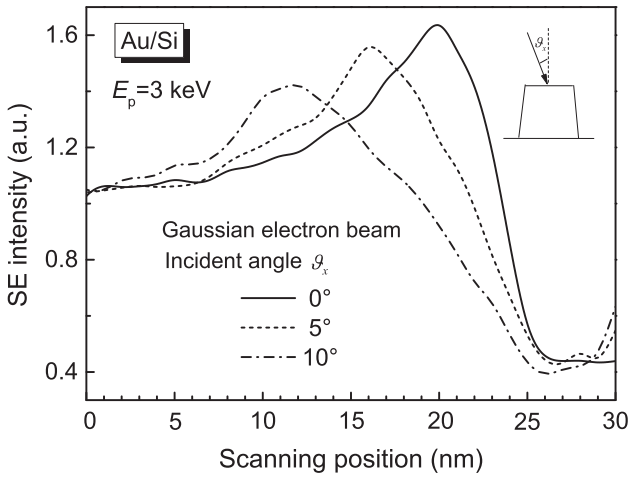


**Fig. 8.** The simulated SE linescan profiles of an Au gate trapezoidal line on a Si substrate under different incident angles of primary electron beam with Gaussian distribution (probe size of 2 nm). The input structure parameters are: $H$ = 50 nm, TCD = 50 nm, SWA = $5^0$; the primary energy is 3 keV.

### 3.3. CD metrology

#### 3.3.1. Pre-processing experimental image

By the MBL method for CD metrology, the SE intensity distribution profile extracted from an experimental CD-SEM image is compared with simulated ones stored in a MBL data file in advance, and then the best fit result will be found to give the CD values. To perform such a matching procedure the experimental image has to be pre-processed by correcting the image orientation, determining the coordinate origin, and normalizing SE linescan curves. The default setting is that the scanning direction is along the positive $x$-axis, and, the centerline of the line structure is along the $y$-axis in the simulation of MBL. However, in the observed SE image of line structure the axis direction of a line may deviate from the $y$-direction; then an automatic operation to judge line direction and make a vertical alignment is necessary. The three steps of pre-processing are rotation of tilted images, selection of the interested field and data normalization.

In the first step, an auxiliary centerline is used to determine the line-axis direction in an image and served as a basis for image rotation. The vertical direction of the corrected image should be aligned to be parallel to the centerline direction. Fig. 10 illustrates the acquisition procedure of auxiliary centerline and image rotation. Fig. 10(a) shows the selected area to be measured in an original CD-SEM image. Firstly, image binarization and edge detection are attained by using the grayscale threshold method and mathematical morphology method in Figs. 10(b) and 10(c), respectively. Secondly, one finds the mean $x$-positions of both outer edges for each vertical $y$-pixels (Fig. 10(d)). These positions are then fitted to a straight centerline as the auxiliary line of image direction, and the slope of the fitted line can be obtained as, $x = ay + b$. Thirdly, if the slope $a$ is greater than a threshold, the image direction needs to be corrected by a rotation operation by an angle according to the slope value such that the fitted centerline becomes parallel to the vertical direction of image frame (Fig. 10(e)). The pixel size is unchanged after image rotation.

In the second step, the field of interest is selected in the CD-SEM image for CD evaluation. It is vertically along the line direction with the length $L$ and is horizontally from the mid of left spacing to the right spacing across over a line structure. The selected area of $(2M + 1) \times N$ pixels, where $N = L/L_p$, the pixel size $L_p$ is calculated based on the scale marker $L_p = L_{scale}/N_{scale}$, where $L_{scale}$ is the "indicator" value (e.g. the nominal value) of the scale marker on the CD-SEM image, $N_{scale}$ is the number of horizontal pixels covering the length of the scale marker. The selected image is then vertically segmented into a series of

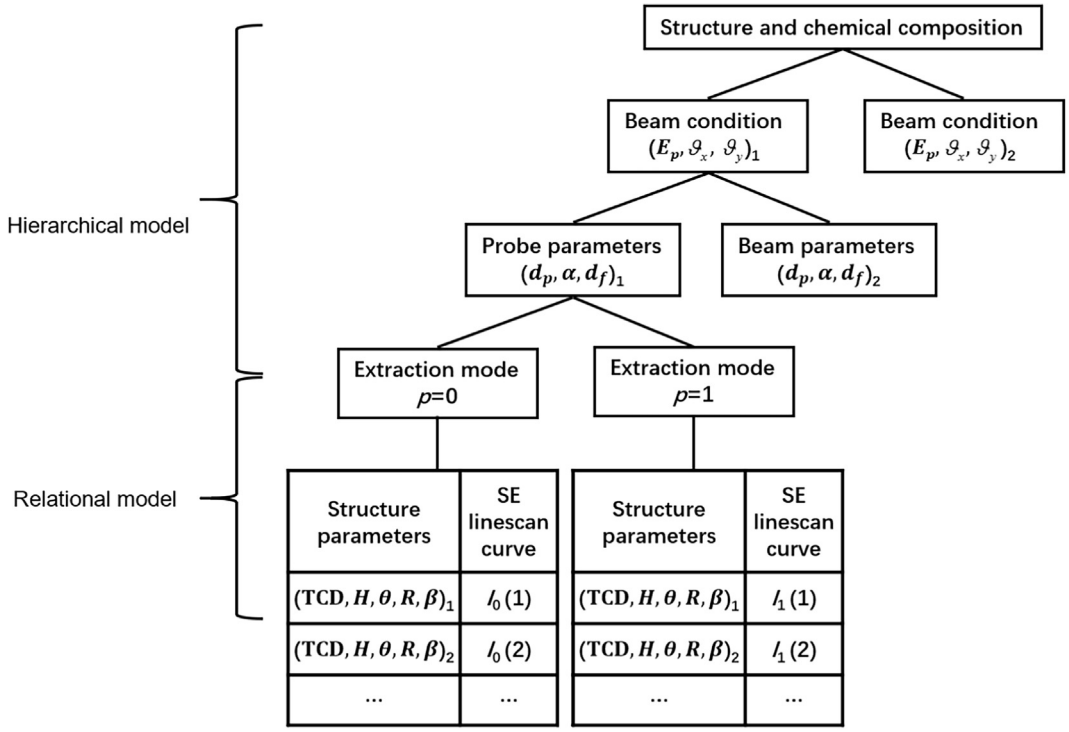


**Fig. 9.** Schematic of data structure for the data file in a MBL database, where $I$ denotes the simulated SE yield curve, $I_k$ ($k$ = 1,2,...,$K$), as a function of horizontal coordinate ($x_k$ = 0,$L_g$,2$L_g$,...,$KL_g$) along scanning direction from center of central line to the mid of right spacing, for a structure parameter set.

horizontal cross-sections with a step length $\Delta L$, and the number of the cross sections is $n = L/\Delta L$ and at least $n > 10$. Usually, $\Delta L = L_p$ and $n = N$ (Fig. 11(a))

To fit with the data in a MBL database, the origin of horizontal coordinate of the line image is set to the center of a line. The horizontal coordinate then becomes $x_i = iL_p$ ($i = -M,...,0,...,M$). The measured SE linescan profiles are then obtained as $I_j(x_i)^{\exp}$ by recording the grayscale intensity for the $j$th ($j$ = 1,...,$n$) vertical cross section. The average of image intensity along the line is then taken to derive the mean measured SE linescan profile (Fig. 11(b)),

$$\bar{I}_i^{\exp} = \frac{1}{n}\sum_{j=1}^{n} I_j(x_i)^{\exp} \quad (i = -M,...,0,...,M). \tag{8}$$

In the third step, the normalization of intensity is done according to the following formula,

$$Y_i^{\exp} = \frac{\bar{I}_i^{\exp} - \bar{I}_{\min}}{\bar{I}_{\max} - \bar{I}_{\min}}, \tag{9}$$

where $\bar{I}_{\min}$ and $\bar{I}_{\max}$ are the minimum and maximum SE emission intensity values of $\bar{I}_i^{\exp}$ ($i = -M, L, 0, L, M$), and $Y_i^{\exp}$ ($i = -M,\ L,\ 0,\ L,\ M$) is the normalized experimental image intensity.

### 3.3.2. MBL data matching

The values of SE signal intensity on each scan position are to be compared between MBL database and the measurement SE image, the same coordinate system should be defined in advance before data matching. However, as the number of horizontal pixels $M$ and pixel size $L_p$ may be different from the number of grid points K and grid size $L_g$ given in a MBL database, an interpolation of experimental image data should be done beforehand to obtain $Y_i^{\exp}$ ($i = -K,...0,...K$) having the

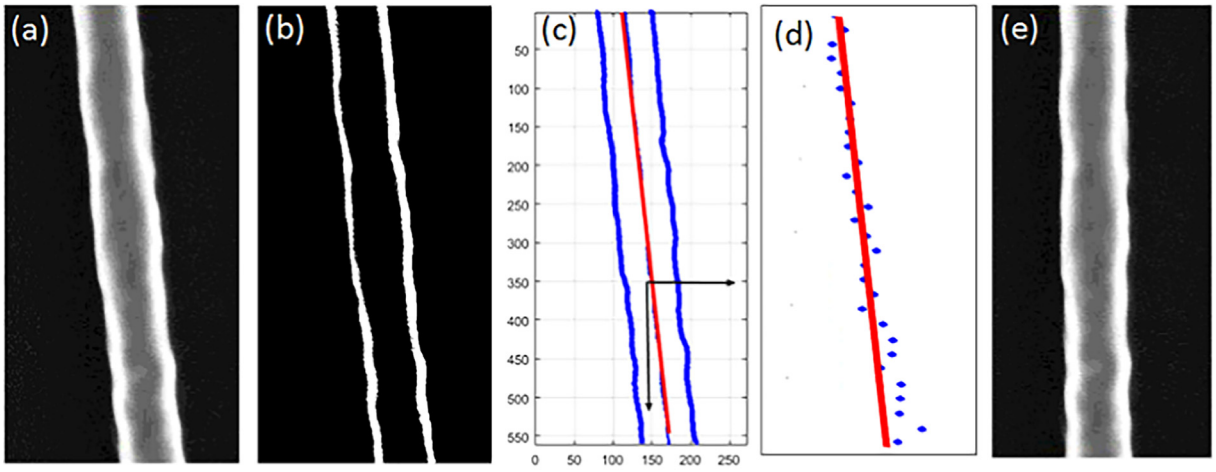


**Fig. 10.** (a) A part of an experimental image; (b) binarized image for outer edge detection; (c) detected outer edges; (d) a linear line fitting of auxiliary center line; (e) corrected image by a rotation.

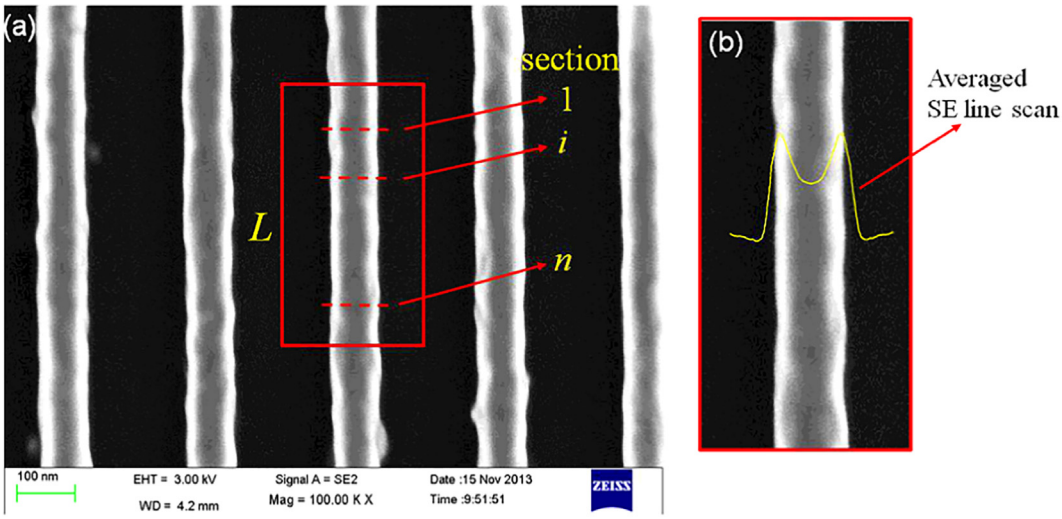


**Fig. 11.** (a) The field of interest is selected with a vertical length $L$ along a line structure in the corrected image, and segmented into a series of cross sections ($i$ = 1,...,$n$) with vertical step length $\Delta L$. (b) SE linescan profiles are obtained by gray scale analysis for each cross section, and averaging is taken to derive mean SE linescan curve.

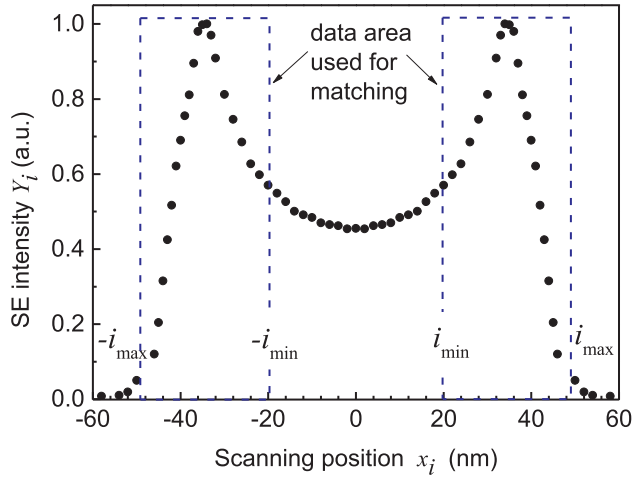


**Fig. 12.** The schematic normalized SE linescan profile extraction from a CD-SEM image. The dashed rectangle represents data area used for MBL matching, for example $T_1 = 0.6$ and $T_2 = 0.05$.

same grid size of $L_g$. Fig. 12 shows a schematic SE linescan profile after intensity normalization and interpolation of horizontal coordinate.

By MBL matching, a least square method is used to for fitting result and searching the optimal CD parameters from a comparison of experimental linescan profile and MBL database. The residual sum of squares in fitting to a single edge on one side (e.g. the right side) of a line is calculated by,

$$\delta = \sum_{i=i_{\min}}^{i_{\max}} (Y_i^{\exp} - Y_i^{\mathrm{MBL}})^2, \tag{10}$$

for asymmetric line, or both sides by

$$\delta = \sum_{i=-i_{\min}}^{-i_{\max}} (Y_i^{\exp} - Y_i^{\mathrm{MBL}})^2 + \sum_{i=i_{\min}}^{i_{\max}} (Y_i^{\exp} - Y_i^{\mathrm{MBL}})^2, \tag{11}$$

for symmetric line, where $i_{\min}$ and $i_{\max}$ are, respectively, the starting (in the edge inner side) and ending (in the edge outer side) grid points for curve matching. As indicated by Fig. 12, the edge position is located in the intensity bloom region, then in matching process we can choose thresholds $T_1$ and $T_2$ for determination of $i_{\min}$ and $i_{\max}$ by $Y_{i_{\min}}^{\exp} > T_1$ and $Y_{i_{\max}}^{\exp} < T_2$, respectively, so that the fitting is performed mainly for the intensity bloom region, where the intensity changes rapidly, in order to reduce the fitting error contributed from the region of insignificance. The MBL linescan profile needs to be also normalized by the similar procedure as given in Eq. (10) or Eq. (11) (after intensity convolution with the Gaussian distribution, Eq. (1), in case of Gaussian probe).

In asymmetric case, this matching will be performed for another side (e.g. the left side) under the same electron beam parameters (primary energy and probe size for a Gaussian probe; primary energy, focus distance and aperture angle for a focusing probe). The optimal fitting results for two sides may be slightly different; we can take an average for TCD and $H$, but SWA, CA and $R$ can be different for two sides. This matching process is repeated for other probe parameters (i.e. probe size for Gaussian probe, or focus distance and aperture angle for focusing probe) and extraction ratio values taking between 0 and 1 so that the best fitting with the least value of residual sum of squares $\delta$ would be found to give the final required CD values.

We have developed a CD-SEM Data Matching Tool (CD-SEM-DMT) to perform such a MBL data matching process. Fig. 13 shows the example matching for SE image of Au pitch features taken by a CD-SEM at an accelerating voltage of 3 kV. The structure is trapezoidal Au lines on a Si substrate. A MBL database including a set of nanostructures and corresponding SE profiles was constructed with conditions as above. The field of interest (red rectangle in Fig. 13) is selected in the CD-SEM image. The matching process was performed by the software CD-SEM-DMT according to the procedure given above. The residual sum of squares $\delta$ reaches a minimum for $T_1 = 0.6$ and $T_2 = 0.05$; we provide in Fig. 13 the SE linescan curves for three structures having the least and better $\delta$-values for a comparison, by assuming a symmetric line shape. The results are then plotted in one figure for visual identification. The corresponding structure in the MBL library represents the measured structure and the CD value is obtained in Table 2.. The BCD is derived from TCD, SWA and $H$, and averaged CD is 94 nm. For a comparison, by the traditional threshold method and setting the edge position as the location of the 50% intensity maxima, the measured distance between the two edges is 84 nm. The threshold method cannot give other structural information.

### 3.3.3. Error analysis for the MBL method

The inherent error of the measurement relates to the principles relied upon. The MBL method based on physical models retains the physical basis of CD-SEM imaging, while the inevitable measurement error is hard to quantify. A model is a mathematical approximation of

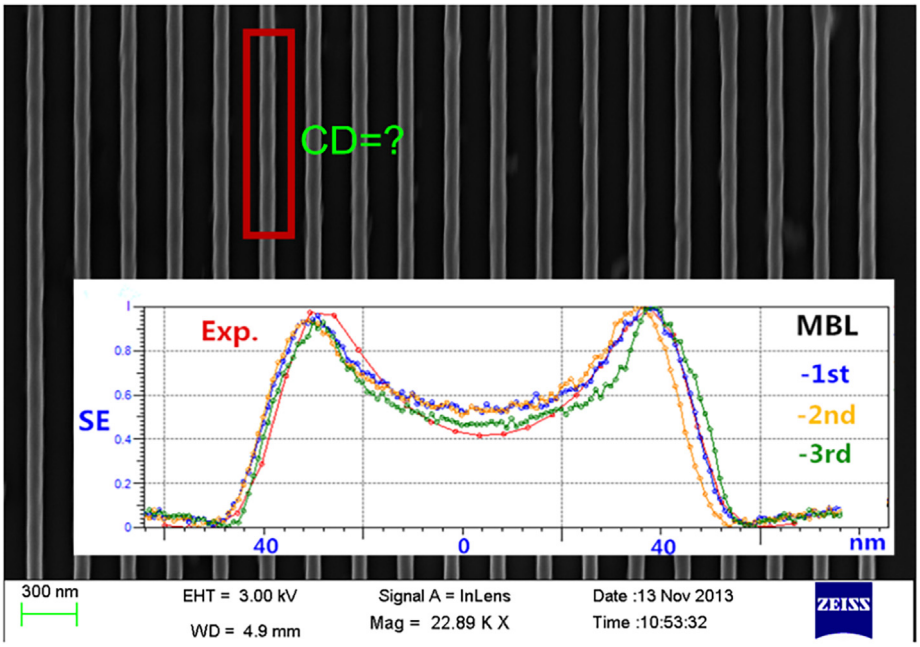


**Fig. 13.** A CD-SEM image of Au lines on a Si substrate at a primary energy of 3 keV, the red rectangle represents the area to be measured. The red dotted line is SE linescan profile deduced from the area on the experimental image, and the remaining three curves are the best and the better matched in MBL.

**Table 2**
The values of structure parameters for an example MBL matching shown in Fig. 12.

| MBL | 1st | 2nd | 3rd |
|---|---|---|---|
| TCD (nm) | 65.0 | 65.0 | 65.0 |
| BCD (nm) | 94.16 | 91.45 | 97.32 |
| Average CD (nm) | 79.58 | 78.23 | 81.16 |
| SWA (deg.) | 11.0 | 10.0 | 13.0 |
| H (nm) | 75.0 | 75.0 | 70.0 |
| $\delta$ | 0.068 | 0.071 | 0.084 |

the physical phenomena and may have incorrect assumptions made by omitting some factors. Different MC physical models can be used to describe the beam-specimen interaction, leading to different SE absolute yields and contrast. The divergence on the physical modeling is one possible source of the measurement errors by the MBL method, especially for the modeling of electron inelastic scattering and SE generation. For example, none of the present MC models have taken into account of SE generation through surface plasmon decay as indicated by a more recent experiment [71]. Furthermore, the charging on the semiconductor surface is still hard to quantify, which depends on many more experimental factors, e.g. beam current density and exposure time [69].

Another important part of the error is due to the structural modeling as the real structure may not be completely described by the structural parameters given in Fig. 2. For example, the surface roughness has not been included in the modeling. In the MC simulation and MBL database construction, one should also pay attention to the resolution of structural parameters, linescan gridding and statistical intensity fluctuation. The more precise structure modeling, higher resolution and less signal noise can reduce this part of error.

In CD evaluation process with the least square method, when the minimum residual sum of squares is reached the best fit CDs are obtained for the optimum modeled structure. However, CDs for other structures may still result in a very similar $\delta$-value. Thus, the matching process may also lead to errors in the measurement. It is suggested to change in this case the thresholds, $T_1$ and $T_2$, to ascertain the more reasonable structure.

## 4. Conclusion

The MBL method according to the relationship between the SE signal waveform and the geometric structure of the specimen and the instrument setup is used in CD metrology by CD-SEM. A model of electron-solid interaction and treating for secondary electrons generation, transport and emission are important for MC simulation in order to build a MBL database. An example MBL database has been constructed and implemented to CD metrology by an up-to-date MC model. Elemental component of the specimen, electron beam condition, probe parameters, signal detection parameter, parameters describing specimen geometry structure, and the corresponding simulated SE profile curves, are stored in the MBL database one by one.

Construction of MBL involves almost the whole process from electron striking the surface of the specimen to SEs emission. The simulated results are affected by many modeling factors, such as, electron scattering model, SE generation model, SE detection model, specimen geometry model. By the MBL method, CD is not just a single variable as line width, but extends to include the detection of 3D topography as specified by many geometry parameters which will be identified from image contrast of a CD-SEM image.The sensitivity of the SE intensity distribution to the structural parameters has been investigated based on the trapezoid with top arcs cross-sectional shape model. The shading effect is taken into account via a SE detector model. The connection of SE signals linescan profile to CD metrology has then built precisely based on the rigorous physics principle that underlies the SE signal formation. We consider that, top CD (TCD), height (H), sidewall angle (SWA, $\theta$), circular angle (CA, $\beta$), and arc radius (R), spacing (d) are necessary geometry parameters, and aperture angle ($\alpha$) and focusing distance ($d_f$) are optional focusing beam parameters for MBL database construction.

We have described in detail the MBL matching procedure. A user-friendly software (CD-SEM Data Matching Tool) was developed for assisting MBL method in CD metrology. The stand-alone off-line MBL database for Au lines on a Si substrate was generated and used to measure CD by the MBL method. SE signal distribution curves were extracted from a selected area in an experimental SE image and matched with results stored in a MBL database. The parameters of geometric structure associated with the best match result represent CD

values of the measured line structure. Compared with the conventional threshold method, the MBL method can obtain more structural information and extends the CD from a single variable as line width to the detection of 3D topography.

## Acknowledgement

This work was supported by the National Natural Science Foundation of China (NSFC) (Nos. 11574289 and 11475215), Fundamental Research Funds for the Central Universities and Special Program for Applied Research on Super Computation of the NSFC-Guangdong Joint Fund (2nd phase) under Grant No. U1501501. Y.G. Li acknowledges the Youth Innovation Promotion Association of Chinese Academy of Sciences (No. 2016386). We also thank the supercomputing center of University of Science and Technology of China for support in performing parallel computations.

## References

[1] H. Morokuma, A. Miyamoto, M. Tanaka, M. Kazui, A. Takane, New technique to reconstruct effective 3D profile from tilt images of CD-SEM, Proc SPIE 5375 (2004) 727–734.
[2] S. Babin, K. Bay, J.J. Hwu, Application of analytic scanning electron microscopy to critical dimensions metrology at nanometer scale, J. Vac. Sci. Technol. B 28 (2010) C6H1–C15.
[3] J.S. Villarrubia, A.E. Vladár, B. Ming, R.J. Kline, D.F. Sunday, J.S. Chawla, S. List, Scanning electron microscope measurement of width and shape of 10 nm patterned lines using a JMONSEL-modeled library, Ultramicroscopy 154 (2015) 15–28.
[4] M.T. Postek, A.E. Vladár, K.P. Purushotham, Does your SEM really tell the truth? How would you know? Part 1, Scanning 35 (2013) 355–361.
[5] M.T. Postek, A.E. Vladár, Modeling for accurate dimensional scanning electron microscope metrology: then and now, Scanning 33 (2011) 111–125.
[6] M.T. Postek, A.E. Vladár, J.S. Villarrubia, A. Muto, Comparison of electron imaging modes for dimensional measurements in the scanning electron microscope, Microsc. Microanal. 22 (2016) 768–777.
[7] W. Häßler-Grohne, D. Hüser, K.-P. Johnsen, C.G. Frase, H. Bosse, Current limitations of SEM and AFM metrology for the characterization of 3D nanostructures, Meas. Sci. Technol. 22 (2011) 94003-1–8.
[8] K. Ueda, S. Koshihara, T. Mizuno, A. Miura, The study of high-sensitivity metrology method by using CD-SEM, Proc. SPIE 7971 (2011) 797124-1–9.
[9] C.G. Frase, E. Buhr, K. Dirscherl, CD characterization of nanostructures in SEM metrology, Meas. Sci. Technol. 18 (2007) 510–519.
[10] J.S. Villarrubia, A.E. Vladár, J.R. Lowney, M.T. Postek, R.A. Allen, M.W. Cresswell, R.N. Ghoshtagore, Linewidth measurement intercomparison on a BESOI sample, Proc. SPIE 3998 (2000) 84–95.
[11] C. Shishido, Y. Takagi, M. Tanaka, Characterizing cross-sectional profile variations by using multiple parameters extracted from top-down SEM images, Proc. SPIE 4689 (2002) 653–660.
[12] T. Onozuka, Y. Ojima, J. Meessen, B. Rijpers, Estimation of pattern shape based on CD-SEM image by using MPPC method, Proc. SPIE 6152 (2006) 61521D-1–9.
[13] B. Bunday, HVM metrology challenges towards the 5nm node, Proc. SPIE 9778 (2016) 97780E.
[14] J.S. Villarrubia, A.E. Vladár, M.T. Postek, A simulation study of repeatability and bias in the CD-SEM, Proc. SPIE 5038 (2003) 138–149.
[15] S. Babin, S. Borisov, A. Ivanchikov, I. Ruzavin, CHARIOT: software tool for modeling SEM signal and e-beam lithography, Phys. Proc. 1 (2008) 305–313.
[16] B. Bunday, A. Cepler, A. Cordes, A. Arceo, CD-SEM metrology for sub-10nm width features, Proc. SPIE 9050 (2014) 90500T-1–20.
[17] C.G. Frase, W. Häßler-Grohne, G. Dai, H. Bosse, Y.A. Novikov, A.V. Rakov, SEM linewidth measurements of anisotropically etched silicon structures smaller than 0.1 μm, Meas. Sci. Technol. 18 (2007) 439–447.
[18] M. Davidson, N. Sullivan, Monte Carlo simulation for CD SEM calibration and algorithm development, Proc. SPIE 2439 (1995) 334–344.
[19] M.P. Davidson, A.E. Vladár, An inverse scattering approach to SEM line width measurements, Proc. SPIE 3677 (1999) 640–649.
[20] D.V. Gorelikov, J. Remillard, N.T. Sullivan, M. Davidson, Model-based CD-SEM metrology at low and ultralow landing energies : implementation and results for advanced IC manufacturing, Surf. Interface Anal. 37 (2005) 959–965.
[21] C.G. Frase, W. Häßler-Grohne, Use of Monte Carlo models in the development and validation of CD operators, Surf. Interface Anal. 37 (2005) 942–950.
[22] C.G. Frase, D. Gnieser, H. Bosse, Model-based SEM for dimensional metrology tasks in semiconductor and mask industry, J. Phys. D: Appl. Phys. 42 (2009) 183001.
[23] J.S. Villarrubia, A.E. Vládar, M.T. Postek, Scanning electron microscope dimensional metrology using a model-based library, Surf. Interface Anal. 37 (2005) 951–958.
[24] J.S. Villarrubia, N.W.M. Ritchie, J.R. Lowney, Monte Carlo modeling of secondary electron imaging in three dimensions, Proc. SPIE 6518 (2007) 65180K-1–14.
[25] J.S. Villarrubia, Z.J. Ding, Sensitivity of SEM width measurements to model assumptions, Proc. SPIE 7272 (2009) 72720R-1–15.
[26] M. Tanaka, C. Shishido, H. Kawada, Influence of electron incident angle distribution on CD-SEM linewidth measurements, Proc. SPIE 6152 (2006) 61523Z-1–11.
[27] M. Tanaka, C. Shishido, W. Nagatomo, K. Watanabe, Application of model-based library approach to Si hardmask measurements, Proc. SPIE 6922 (2008) 69222L-1–11.
[28] M. Tanaka, J.S. Villarrubia, A.E. Vladár, Influence of focus variation on linewidth measurements, Proc. SPIE 5752 (2005) 144–155.
[29] S. Babin, S. Borisov, A. Ivanchikov, I. Ruzavin, Modeling of linewidth measurement in scanning electron microscopes using advanced Monte Carlo software, J. Vac. Sci. Technol. B 24 (2006) 3121–3124.
[30] A. Karabekov, O. Zoran, Z. Rosenberg, G. Eytan, Using monte carlo simulation for accurate critical dimension metrology of super small isolated poly-lines, Scanning 25 (2003) 291–296.
[31] M. Ciappa, A. Koschik, M. Dapor, W. Fichtner, Modeling secondary electron images for linewidth measurement by critical dimension scanning electron microscopy, Microelectr. Reliab. 50 (2010) 1407–1412.
[32] Y.G. Li, P. Zhang, Z.J. Ding, Monte Carlo simulation of CD-SEM images for linewidth and critical dimension metrology, Scanning 35 (2013) 127–139.
[33] N. Yasui, M. Isawa, T. Ishimoto, K. Sekiguchi, M. Tanaka, M. Osaki, C. Shishido, N. Hasegawa, S. Cheng, Application of model-based library approach to photoresist pattern shape measurement in advanced lithography, Proc. SPIE 7638 (2010) 76382O-1–11.
[34] M. Isawa, M. Tanaka, H. Kazumi, C. Shishido, A. Hamamatsu, N. Hasegawa, P. De Bisschop, D. Laidler, P. Leray, S. Cheng, Verification and extension of the MBL technique for photo resist pattern shape measurement, Proc. SPIE 7971 (2011) 79710Z-1–11.
[35] C. Shishido, M. Tanaka, M. Osaki, CD bias reduction in CD-SEM line width measurement for 32nm node and beyond by using model-based library method, Proc. SPIE 7272 (2009) 72722C-1–10.
[36] V. Khvatkov, V. Alievski, R. Kadushnikov, S. Babin, Automated metrology for SEM calibration and CD line measurements using image analysis and SEM modeling methods, Proc. SPIE 6922 (2008) 69222N-1–12.
[37] A.E. Vladár, J.S. Villarrubia, J. Chawla, B. Ming, J.R. Kline, S. List, M.T. Postek, 10nm three-dimensional CD-SEM metrology, Proc. SPIE 9050 (2014) 90500A.
[38] S.F. Mao, Y.G. Li, R.G. Zeng, Z.J. Ding, Electron inelastic scattering and secondary electron emission calculated without the single pole approximation, J. Appl. Phys. 104 (2008) 114907-1–10.
[39] Y.G. Li, S.F. Mao, H.M. Li, S.M. Xiao, Z.J. Ding, Monte Carlo simulation study of scanning electron microscopy images of rough surfaces, J. Appl. Phys. 104 (2008) 64901-1–7.
[40] J.S. Villarrubia, A.E. Vladár, M.T. Postek, 3D Monte Carlo modeling of the SEM: are there applications to photomask metrology? Proc. SPIE 9236 (2014) 923602-1–12.
[41] R. Shimizu, Z.J. Ding, Monte Carlo modelling of electron-solid interactions, Rep. Prog. Phys. (1992) 487–531.
[42] Z.J. Ding, R. Shimizu, A Monte Carlo modeling of electron interaction with solids including cascade secondary electron production, Scanning 18 (1996) 92–113.
[43] Z.J. Ding, H.M. Li, Application of Monte Carlo simulation to SEM image contrast of complex structures, Surf. Interface Anal. 37 (2005) 912–918.
[44] Z.J. Ding, H.M. Li, X.D. Tang, R. Shimizu, Monte Carlo simulation of absolute secondary electron yield of Cu, Appl. Phys. A 78 (2004) 585–587.
[45] P. Zhang, H.Y. Wang, Y.G. Li, S.F. Mao, Z.J. Ding, Monte Carlo simulation of secondary electron images for real sample structures in scanning electron microscopy, Scanning 34 (2011) 145–150.
[46] Y.B. Zou, S.F. Mao, B. Da, Z.J. Ding, Surface sensitivity of secondary electrons emitted from amorphous solids: calculation of mean escape depth by a Monte Carlo method, J. Appl. Phys. 120 (2016) 235102-1–12.
[47] Z. Ruan, P. Zhang, S.F. Mao, H.M. Li, Z.J. Ding, Monte Carlo study of the influence of electron beam focusing to SEM image sharpness measurement, e-J Surf. Sci. Nanotech. 2 (2014) 247–251.
[48] Z. Ruan, S.F. Mao, P. Zhang, H.M. Li, Z.J. Ding, Monte Carlo simulation of realistic beam-sample interaction in SEM: application to evaluation of sharpness measurement methods, Proc. SPIE 8729 (2013) 87290J1-14.
[49] A. Kyritsakis, J.P. Xanthakis, Beam spot diameter of the near-field scanning electron microscopy, Ultramicroscopy 125 (2013) 24–28.
[50] T. Radlička, Wave optical calculation of probe size in low energy scanning electron microscope, Microsc. Microanal. 21 (2015) 212–217.
[51] K. Hitomi, Y. Nakayama, H. Yamanashi, Y. Sohda, H. Kawada, Study of measurement condition optimization in critical dimension-scanning electron microscope, Jpn. J. Appl. Phys. 47 (2008) 6554–6557.
[52] E. Solecky, C. Archie, J. Mayer, R. Cornell, O. Adan, Characterizing and understanding stray tilt: the next major contributor to CD SEM tool matching, Proc. SPIE 5038 (2003) 518–527.
[53] P. Zhang, S.F. Mao, Z.M. Zhang, Z.J. Ding, Monte Carlo study of the influence of electron beam focusing to SEM linewidth measurement, Proc. SPIE 8729 (2013) 87290K.
[54] M. Sato, T. Ogashiwa, Relation between optimal focus condition and a pixel size or an image magnification in a digital SEM, Phys. Proc. 1 (2008) 127–133.
[55] M. Sato, Properties of the imaging performance of an electron optical system for SEM, Nucl. Instrum. Meth. Phys. Res. A 645 (2011) 74–78.
[56] J. Cazaux, Recent developments and new strategies in scanning electron microscopy, J. Microsc. 217 (2005) 16–35.
[57] M.S. Bronsgeest, J.E. Barth, L.W. Swanson, P. Kruit, Probe current, probe size, and the practical brightness for probe forming systems, J. Vac. Sci. Technol. B 26 (2008) 949–955.
[58] Z.J. Ding, Z.Q. Wu, A comparison of Monte Carlo simulations of electron scattering and X-ray production in solids, J. Phys. D: Appl. Phys. 26 (1993) 507–516.
[59] Y.T. Yue, H.M. Li, Z.J. Ding, Monte Carlo simulation of secondary electron and

backscattered electron images in scanning electron microscopy for specimen with complex geometric structure, J. Phys. D: Appl. Phys. 38 (2005) 1966–1977.
[60] Z. Ruan, R.G. Zeng, Y. Ming, M. Zhang, B. Da, S.F. Mao, Z.J. Ding, Quantum trajectory Monte Carlo method for study of electron-crystal interaction in STEM, Phys. Chem. Chem. Phys. 17 (2015) 17628–17637.
[61] N.F. Mott, The scattering of fast electrons by atomic nuclei, Proc. R. Soc. London A124 (1929) 425–442.
[62] R.A. Bonham, T.G. Strand, Analytical expressions for potentials of neutral Thomas-Fermi-Dirac atoms and for the corresponding atomic scattering factors for x-rays and electrons, J. Chem. Phys. 39 (1963) 2200–2204.
[63] Y. Yamazaki, Studies on Electron Scattering by Mercury Atoms and Electron Spin Polarization Detector (Ph.D. thesis, Osaka University), 1977.
[64] D.R. Penn, Electron mean-free-path calculations using a model dielectric function, Phys. Rev. B 35 (1987) 482–486.
[65] E.D. Palik, Handbook of Optical Constants of Solids, Academic Press, New York, 1998.
[66] B.L. Henke, E.M. Gullikson, J.C. Davis, X-ray interactions: Photoabsorption, scattering, transmission, and reflection at $E = 50–30{,}000$ eV, $Z = 1–92$, At. Data Nucl. Data Tables 54 (1993) 181.
[67] C. Cohen-Tannoudji, B. Diu, F. Laloe, Quantum Mechanics, Hermann, Paris, 1977.
[68] Z.J. Ding, X.D. Tang, R. Shimizu, Monte Carlo study of secondary electron emission, J. Phys. D: Appl. Phys. 89 (2001) 718–726.
[69] C. Li, S.F. Mao, Y.B. Zou, Y.G. Li, P. Zhang, H.M. Li, Z.J. Ding, A Monte Carlo modeling on charging effect for structures with arbitrary geometries, J. Phys. D: Appl. Phys. (2018) (in press).
[70] P. Zhang, H.Y. Wang, Y.G. Li, S.F. Mao, Z.J. Ding, Monte Carlo simulation of secondary electron images for real sample structures in scanning electron microscopy, Scanning 34 (2012) 145–150.
[71] W.S.M. Werner, F. Salvat-Pujol, A. Bellissimo, R. Khalid, W. Smekal, M. Novák, A. Ruocco, G. Stefani, Secondary-electron emission induced by in vacuo surface excitations near a polycrystalline Al surface, Phys. Rev. B 88 (2013) 201407(R).